USIP -- 82 - 03.

NUCLEAR MOLECULAR STRUCTURE IN HEAVY MASS SYSTEMS

T. Arctaedius and Chr. Bargholtz
Department of Physics, University of Stockholm, Vanadisvägen 9,
S-113 46 Stockholm, Sweden

Abstract

A study is made of nuclear molecular configurations involving one heavy mass partner. The stability of these configurations to mass flow and to fission is investigated as well as their population in fusion reactions. It is concluded that shell effects in combination with the effects of angular momentum may be important in stabilizing certain configurations. A possible relation of these configurations to the so called superdeformed states is pointed out.

The spectrum of rotational and vibrational transitions within molecular configurations is investigated. For sufficiently mass-asymmetric systems the energies of vibrational transitions are comparable to the neutron separation energy. Gamma radiation from such transitions may then be observable above the background of statistical transitions. The gamma spectrum and the directional distribution of the radiation following fusion reactions with ^{12}C and ^{16}O are calculated.

1. Introduction

In the first scattering experiments made with heavy-ion projectiles, back in 1960, an unexpected intermediate structure, was observed both for beam energies close to the Coulomb barrier and for energies well above the barrier [1]. This "resonance" or intermediate structure in the reaction cross section was explained as being due to the formation of an intermediate, dinuclear, state with comparatively long lifetime. The decay paths open for such a dinuclear state would be the formation of a compound system or the break up into two separate systems. Observations of this effect in scattering experiments are ample, though only for relatively light systems; $^{12}C+^{12}C$, $^{12}C+^{16}O$ and $^{16}O+^{16}O$ [2]. Molecular effects have also been observed in the $^{12}C+^{13}C$ exit channel of the reaction $^{16}O+^{9}Be$ [3]. Calculations are also often restricted to light systems. Experiments trying to observe the gamma radiation originating from the "molecular" state have been made, using the reaction $^{12}C(^{12}C,\gamma)^{24}Mg$ [4], but so far molecular gamma transitions have not been unambiguously identified.

To study the electromagnetic properties of the dinuclear state, we have calculated the energies and transition probabilities for vibrational and rotational electromagnetic transitions within a rotating molecule-like configuration. The time dependence has been studied by means of a Monte Carlo random walk simulation.

We begin, in section two, with a description of a simple model used for the calculation of energies, wave functions of the molecular states and electromagnetic transition probabilities. Some general results are presented as well. The stability of the dinucleus against mass exchange and fission is then discussed in section three. The question of the population of excited molecular states in heavy-ion fusion reactions is addressed in section four, followed, in section five, by a discussion of the results for two particular systems, $^{12}C + ^{159}Tb$ and $^{16}O + ^{208}Pb$, and their relation to experimental results. Finally, in section six, we discuss the implications of the present model on fusion-fission reactions and point out a possible connection between the molecular configurations of the present approach and the so called superdeformed states.

2. A model for dinuclear states.

2.1 Calculation of energies and transition probabilities.

The dinuclear state is supposed to be formed when the incoming ion is trapped in the secondary potential minimum, which naturally arises when the Coulomb, nuclear and centrifugal forces between the two ions are added (cf. Fig 1). In order to describe the states one thus needs an expression for the potential acting between two heavy ions.

A multitude of descriptions of the ion-ion potential have been attempted. Most of the potentials are folding potentials, i.e. they are derived by folding the potential for the scattering of

a nucleon in the field of one of the nuclei with the density distribution of the other nucleus. When the distance between the nuclei is smaller than the sum of the radii, there are different possibilities how to treat the overlap of matter. The two extreme approaches are the adiabatic and the sudden approximations. In the adiabatic approximation the total volume is conserved and no compression occurs. This approximation is mostly used when the energies are low. In the sudden approximation the densities are added resulting in a strong repulsion at small distances, which can be regarded as an effect of the Pauli principle.

We have used a potential calculated in the sudden approximation using the energy density formalism and a parametrization of Ngô *et al.* [5].

$$V_N(r_{12}) = \frac{A_1^{1/3} A_2^{1/3}}{A_1^{1/3} + A_2^{1/3}} U_n$$

$$U_n = \begin{cases} -V_0 e^{-0.27 s^2} & s \geq 0 \\ -V_0 + 6.3 s^2 & s < 0 \end{cases}$$

where

$$s = r_{12} - R_1 - R_2$$

and

$$V_0 = 30 \text{ MeV}.$$

The radii were taken to be $R_i = r_0 A^{1/3}$ with r_0=1.0 fm and r_{12} is the distance between the two ions. This parametrization works well for systems with atomic numbers, Z_1 and Z_2, such that $300 \leq Z_1 Z_2 \leq 4000$. No correction for shell effects was made. To test the sensitivity of the results to the choice of potential the calculations were repeated with the proximity potential [6]. This did not change the results significantly.

The situation is somewhat more complicated for deformed nuclei. In order to be able to treat the problem one-dimensionally we have used the equivalent spheres approximation for deformed nuclei. This method has been used to incorporate the effects of deformation in calculations of sub-barrier fusion cross sections [7]. The approximation treats the deformed nucleus by replacing it with a series of spherical nuclei of different radii. The radius of the deformed nucleus was taken to be $R(\theta) = r_0 A^{1/3}(1 + \beta_2 Y_{20}(\theta))$, where β_2 is the deformation parameter. The potential is then averaged over all angles of orientation to get an effective potential,

$$V_{\text{eff}}(r_{12}) = \int_0^{\pi/2} V(\theta, r_{12}) \sin\theta d\theta.$$

Fig 1 shows an example of the total potential (nuclear + Coulomb + centrifugal) for different angular momenta.

We have calculated the spectrum of dinuclear excitations by solving the one dimensional time-independent Schrödinger equation for the ion-ion potential. This was done by fitting a harmonic oscillator potential to the pocket in the ion-ion potential. The corresponding (displaced) harmonic oscillator wave functions were then used as a set of basis states together with standard angular momentum eigen functions when diagonalizing the total Hamiltonian.

2.2 General results of the model.

Displayed in Fig 2 is the calculated spectrum of molecular excitations for a range of orbital angular momenta. The levels are grouped into the characteristic rotational bands of molecular spectroscopy.

The electromagnetic transitions connecting the levels in Fig 2 are basically of two kinds, rotational transitions with an energy below approximately 2 MeV and vibrational transitions with an energy between 5 and 10 MeV. Within the rotational bands, the dominant transitions are of electric dipole character. The vibrational transitions are of both electric dipole and electric quadrupole character, quadrupole transitions dominating at the higher energies. The reduced transition probabilities are given by

$$B(E\lambda) = e^2_{\mathrm{eff}_\lambda} |\langle I_f \| Y_\lambda \| I_i \rangle|^2 |\langle j_f | r^\lambda | j_i \rangle|^2$$

where

$$e_{\mathrm{eff}_1} = e \frac{A_{target} Z_{beam} - A_{beam} Z_{target}}{A_{target} + A_{beam}}$$

and

$$e_{\mathrm{eff}_2} = e Z_{beam}.$$

For the higher energies stretched quadrupole transitions dominate, while for lower energies the dominant transitions are non-stretched ($\Delta I = 0$) quadrupole transitions. This means that there is a drastic change in the directional distribution coefficient A_2 with energy: the A_2 coefficient is +0.32 for non-stretched and -0.32 for stretched E2 transitions.

Fig 3 shows the calculated energy for the first vibrational transition, $\nu = 1 \rightarrow \nu = 0$, at an orbital angular momentum L=15, for different target/beam combinations. The energy of the vibrational transitions is higher for more asymmetric systems. The gamma ray spectrum from the decay of hot compound nuclei shows an exponential decrease in intensity up to the neutron separation energy ($\sim$ 8-10 MeV) and then a shoulder corresponding to the deexcitation of the GDR in the hot compound nucleus. To observe the molecular gamma-ray transitions, created in heavy-ion reactions, experimentally, one should thus study asymmetric systems and preferable measure directional distributions.

3. Life time of dinuclear states.

A crucial point in any discussion of nuclear molecular states is their stability against decay by other means than electromagnetic transitions. In the model discussed in the previous section the main decay modes are: tunneling through the outer barrier, mass flow to the heavier partner resulting, eventually, in compound nucleus formation, and, at least for systems with one very heavy constituent nucleus, fission of the heavier partner.

We have investigated the life time of certain dinuclear configurations by means of a Monte Carlo calculation including statistical neutron emission from the constituent nuclei in addition to the three decay channels above.

The tunneling probability increases with orbital angular momentum and vibrational excitation energy. For a given mass division the probability increases with increasing Coulomb energy between the two nuclei, i.e. for a more equal charge division. We have calculated the tunneling probability, $\lambda_{tunnel}(Z_1, A_1, Z_2, A_2, \nu, L)$, for a given molecular state in the JWKB approximation [8]

$$\lambda_{tunnel} = \frac{exp\{-\frac{\sqrt{8\mu}}{\hbar}\int_{TP_2}^{TP_3}[V - E_{\nu,L}]^{1/2}dr_{12}\}}{\sqrt{2\mu}\int_{TP_1}^{TP_2}[E_{\nu,L} - V]^{-1/2}dr_{12}}$$

In this expression TP_1, TP_2 and TP_3 denote the three classical turning points, in order of increasing radius, at total energy $E_{\nu,L}$, $V(Z_1, A_1, Z_2, A_2, r_{12})$ is the ion-ion potential and μ is the reduced mass. Due to the depth of the pocket in the ion-ion potential, the effect of tunneling through the outer barrier is of minor importance, even for the ν=2 state at an intermediate angular momentum.

In our investigation of the mass flow between the two nuclei we have followed the treatment of Ayik, Schürman and Nörenberg [9], however, inserting instead of liquid drop masses for the constituent nuclei, measured ground state masses or mass predictions [10] and including the total calculated molecular energy in place of only the schematic rotational and Coulomb energies.

The transport of nucleons between the two nuclei can be divided into a diffusive process, increasing with temperature, and a mass drift governed by the so called driving potential , $U(Z_1, A_1, Z_2, A_2, \nu, L)$. Apart from corrections due to nuclear structure introduced through the use of "realistic" ground state masses the driving potential is such that for strongly mass-asymmetric systems and low angular momentum it tends to increase the asymmetry eventually leading to compound nucleus formation. The flow rate decreases with increasing angular momentum until it is finally reversed. The introduction of shell effects into the driving potential may strongly influence the mass drift, changing this picture altogether in particular for low nuclear temperatures. The driving potential is illustrated in Figure 4 for

the system A=171, Z=71 for symmetries in the vicinity if the system $^{12}C + ^{159}Tb$. In our calculation the probability for a proton to make the transition from nucleus one to nucleus two, $\lambda_z(Z_1, A_1, Z_2, A_2, \nu, L)$, was given by

$$\lambda_z = 3 \cdot 10^{22} \frac{Z_1 + Z_2}{A_1 + A_2} \left(\frac{E_{cm} - U}{g_1 + g_2} \right)^{1/4} \left(\frac{g_1^{1/3} g_2^{1/3}}{g_1^{1/3} + g_2^{1/3}} \right)^2 \left(1 + \frac{\Delta U}{T} \Theta(\Delta U) \right) s^{-1}$$

where

$$\Delta U = U(Z_1, A_1, Z_2, A_2, \nu, L) - U(Z_1 - 1, A_1 - 1, Z_2 + 1, A_2 + 1, \nu, L)$$

and

$$\Theta(x) = \begin{cases} 1 & x > 0 \\ 0 & x \leq 0 \end{cases}$$

The modifications in the case of a neutron are obvious. In this expression E_{cm} denotes the total initial center of mass energy (including masses), lowered by the energy carried off by evaporated neutrons. The driving potential, $U(Z_i, A_i, Z_j, A_j, \nu, L)$, equals the total energy of the state with molecular quantum numbers ν and L and the constituent nuclei (Z_i, A_i) and (Z_j, A_j) in their ground states. The nuclear temperature is taken to be

$$T \equiv \sqrt{(E_{cm} - U)/a}$$

and

$$a \approx g_1 + g_2.$$

For the single particle level densities we used, $g_i = A_i/8$. For all other parameters, collected in the numerical coefficient we have adopted the values used in ref. [9]. All energies are measured in MeV.

For such dinuclear systems where one of the constituents is a very heavy nucleus, say in the lead region or above, fission of the heavier partner can be an important decay mechanism, strongly dependent on the internal angular momentum of that nucleus. In the present calculation we have used the standard theory of Bohr and Weeler neglecting any influence from the nearby charge:

$$\frac{\Gamma_F}{\Gamma_N} = \frac{\sqrt{(4\sqrt{a}\sqrt{E_i^* - B_F} - 2)\, e^{(2\sqrt{a}(\sqrt{E_i^* - B_F} - \sqrt{E_i^* - B_N}))}}}{2\sqrt{a}\sqrt{E_i^* - B_N} - 1}$$

where B_N is the neutron binding energy.

The internal excitation energy, was taken to be

$$E_i^* \equiv \frac{A_i}{(A_1 + A_2)}(E_{cm} - U).$$

For the height of the fission barrier, B_F we used the liquid drop estimate lowered by a factor of 0.6 [2]. The level density parameter was assumed to remain unchanged at the saddle point.

Due to the heating of the constituent nuclei, neutrons will be evaporated from the dinucleus. The probability for neutron emission from the constituent nucleus i was taken to be

$$\frac{1}{\lambda_N} = \frac{2mR^2}{\pi\hbar^3}\frac{1}{a}(E_i^* - B_N)\, e^{2\sqrt{a}(\sqrt{(E_i^* - B_N)} - \sqrt{E_i^*})}$$

Using the transition probabilities above we performed Monte Carlo calculations of the time development of ensembles of certain nuclear molecules. We concentrated on such asymmetric systems for which the electromagnetic transition energies are sufficiently high to make them observable. A general result was that there is a delicate balance of counteracting tendencies. In the lower vibrational states, and in particular for low angular momenta, the system developes rapidly towards the compound nucleus. At higher angular momenta "molecular" life times may be of the order of 10^{-20}s. For the more long-lived configurations there is often a development towards increased symmetry. Shell effects play an important role in stabilizing certain dinuclear configurations. As an example the time development of the mass asymmetry is illustrated in Figure 5 for a system starting out as $^{12}C + {}^{159}Tb$ at an intermediate angular momentum.

4. Population of molecular states.

In order to make predictions concerning the possibility to observe electromagnetic transitions between nuclear molecular states we need a model for their population. The most obvious way to populate the states is by means of heavy-ion fusion reactions. However, the overwhelming complexity of the reaction mechanism makes it necessary to simplify the problem considerably. In order to calculate the relative population of molecular vibrational states with a given orbital angular momentum we have devised the following model.

The asymptotic two body wave function in the initial channel was chosen in such a way as too correspond to a totally absorbed wave:

$$\psi_{asymptot} \propto F_L(kr_{12}) + iG_L(kr_{12})$$

where F and G are the regular and irregular solutions to the pure Coulomb problem. We then integrated the Schrödinger equation inwards starting well outside the nuclear potential, with the asymptotic solution as a boundary condition. We neglected the coupling between the collective orbital angular momentum, L, and the internal angular momentum, the spin, of the two nuclei. The Schrödinger equation could then be separated. It is not possible, however, to neglect the coupling of the radial motion to the internal excitation of the two nuclei. Attempting to integrate the Schrödinger equation with the real molecular potential alone does not lead to an acceptable solution for the scattering wave function, $\psi_L^{in}(r_{12})$. Instead an imaginary potential has to be included to take care of the absorption. We did not experiment with different shapes for the imaginary potential but took it to be directly proportional to the overlap of the two nuclei

$$W(r_{12}) = const \cdot \int \rho_1 \rho_2 dV$$

with

$$\rho_i = \rho_0[1 + e^{(r-0.93R_i)/0.6}]^{-1}$$

The strength of the potential was chosen as the minimum required to make the two body wave function go smoothly to zero at about the inner classical turning point. As it turned out this requirement made the strength of the (attractive) imaginary potential increase smoothly with center of mass energy.

The relative population of the different molecular vibrational states was then taken as proportional to the square of the matrix element of the imaginary potential between the incoming wave and the bound state wave functions, $\psi_{\nu L}$.

$$Population(\nu) \propto |\langle \psi_{\nu L} \mid W(r_{12}) \mid \psi_L^{in} \rangle|^2$$

A general feature of the calculated relative population probabilities is that the ground state is very weakly populated. For the excited vibrational states the population increases with increasing energy. The results change only slowly with angular momentum and laboratory energy. The resulting relative population probabilities in two specific reactions are discussed in section 5.

5. Molecular systems of $^{12}C + ^{159}Tb$ and $^{16}O + ^{208}Pb$.

We have investigated two dinuclear systems a little more in detail. These particular examples are chosen because experimental data exist for them which point to the possibility that gamma radiation from molecular transitions may have been observed.

For the $^{12}C + ^{159}Tb$ system the gamma ray spectrum following fusion reactions has been measured at a beam energy of 100 MeV [11]. At this energy the average angular momentum of the fusion channel is approximately $33\hbar$. Assuming a situation in between that of rolling and sliding we have made our calculations at an orbital angular momentum, L = 15 $\hbar$. Our result for the population of the various vibrational levels shows that the ground state is populated directly in less than two per cent of all reactions. In our model the main part of the fusion reactions, approximately 80 per cent, proceed through capture to the second excited vibrational state. Higher lying states contribute to the deep inelastic cross section. The time development of the mass asymmetry for the second excited vibrational state is illustrated in Figure 5. The lifetime of the state is approximately $4.5 \cdot 10^{-21}$s. These results change only slowly with orbital angular momentum.

From the calculated relative population probabilities and life times the gamma ray spectrum from molecular transitions could be calculated. An effective mass of 0.85 was assumed for the ^{12}C nucleus. This does not change the transition probabilities, it only shifts the energy of the transitions. The resulting spectrum is shown in fig 6 together with the measured total gamma-ray spectrum from the $^{12}C+^{159}Tb$ reaction at E_{lab} = 100 MeV. The main part of the spectrum is due to the statistical decay of the compound nucleus. We have not attempted any fit to the measured gamma-ray spectrum in this case, due to the large uncertainties in the parameters of the giant dipole resonance which affect the spectral shape in the region of the molecular transitions. For any resonable set of parameters, however, the directional distribution of the gamma rays from the compound nucleus is nearly isotropic in this region of the spectrum and changes only slowly with energy. In contrast, the directional distribution of gamma rays from molecular transitions is predicted to change rapidly with energy.

In fig 7 the calculated directional distribution coefficients are compared to the measured ones. One observes that the experimental values show the change in sign of the coefficient expected for molecular transitions.

In an experiment at Stony Brook, Thoennessen *et al.* [12], and [13], observed an enhanced emission of gamma rays with energies between 8 and 13 MeV following fusion reactions of ^{16}O and ^{208}Pb. At laboratory energies of 100, 120, and 140 MeV the gamma-ray spectrum above 13 MeV was associated with the decay of the giant dipole resonance in the hot fission fragments. In the energy region between 8 and 13 MeV an increased emission rate was observed as compared to the result of a statistical model calculation. The authors interpreted this excess gamma radiation as being due to a hindrance of the fission channel leading to an increased pre-fission decay of the giant dipole resonance in the hot compound nucleus. The spectrum calculated within a statistical model (CASCADE) was brought into agreement with the observed one by assuming a strong hindrance of the fission channel in the first few steps of the statistical cascade.

We have made a calculation for the $^{16}O+^{208}Pb$ system similar to the one for $^{12}C+^{159}Tb$. At a laboratory energy of 120 MeV we arrive at approximately the same value for the orbital angular momentum of the dinucleus. The results of the calculation are that the relative population of the vibrational states is approximately the same as in the C+Tb case, but that the lifetime is slightly shorter, $3 \cdot 10^{-21}$ s. With an effective mass of 0.8 for ^{16}O the observed gamma ray spectrum is well reproduced, between 8 and 13 MeV, by adding the molecular yield to the statistical yield including the GDR, assuming no hindrance of the fission off the compound nucleus. Fig 8 shows the result of the calculation together with the measured spectrum.

6. Discussion.

The results of our investigation show that vibrational transitions in mass asymmetric nuclear molecular configurations may contribute significantly to the gamma ray spectrum from certain heavy-ion reactions. Even though a combination of shell effects and effects of angular momentum tend to stabilize the dinucleus, this gamma-ray source is a weak one. Instead its significance lies in the fact that the gamma-ray energy falls in between that of the statistical transitions feeding the yrast region and the giant dipole resonance, an otherwise relatively weak and structureless part of the spectrum. Too much emphasis must not be placed on the detailed outcome of the comparisons made to measured spectra and directional correlation coefficients, however. As pointed out above the parameters used in the statistical model calculations, including level densities and GDR parameters, are rather uncertain. Also, in our calculation of the C+Tb and O+Pb systems, the effective mass plays the role of an undetermined parameter. Although the value assumed seems in no way unreasonable, this point should be paid further attention.

It should be pointed out what seems to be a relation between the location of the minimum in the driving potential for the higher angular momenta (cf. Figure 4) and the so called superdeformed states. For the vibrational ground state at I = 30 this minimum occurs for $A1/A2 \approx 0.2$. Computing the value of β_2 in the corresponding configuration we find $\beta_2 = 0.7$. A value compatible with a ratio of major- to minor axes of 2:1.

In our calculation of the $^{16}O + ^{208}Pb$ system fission is delayed by approximately the life time of the molecular states. Fission of the heated heavy mass partner occurs but is rare ($\approx$1% of all cases). This mechanism for fission delay is quite different from those discussed by Gavron *et al.* [14] — the finite time until equilibrium fission probability is attained at the saddle point and the effects of nuclear viscosity. However, the resulting time delay is of the same magnitude. The possible formation of intermediate nuclear molecular configurations, therefore, may influence appreciably the characteristics of the so called fusion-fission reactions.

We owe thanks to Dr Per-Erik Tegnér for his contribution during this initial phases of the investigation. This work was supported by the Swedish Natural Science Research Council.

REFERENCES

[1] E. Almqvist, D.A. Bromley and J.A. Kuehner, Phys. Rev. Lett. 4(1960)515.

[2] R. Bass, Nuclear Reactions with Heavy Ions (Springer, Berlin 1980) and references therein.

[3] I. Weitzenfelder, N. Bischof, W. Tiereth, H. Voit, W von Oertzen and H.H. Wolter, Nucl. Phys. A489(1988)125.

[4] B. Dechant and E. Kuhlmann, Z. Phys. A330(1988)93.

[5] C. Ngô, B. Tamain, M. Beiner, R.J. Lombard, D. Mas, and H.H. Deubler, Nucl Phys. A252(1975)237

[6] J. Blocki, J. Randrup. W.J. Swiatecki, and C.F. Tsang Ann. Phys. 105(1977)427

[7] R.G. Stokstad and E.E. Gross, Phys. Rev. C23(1981)281

[8] N. Elander, M Hehenberger and P.R. Bunker, Physica Scripta, 20(1979)631.

[9] S. Ayik, B. Schürmann and W Nörenberg, Z. Phys. A279(1976)145

[10] 1986-1987 Atomic Mass Predictions, ed. P.E. Haustein, Atomic Data and Nuclear Data Tables 39(1988)185.

[11] Th. Arctaedius, Chr. Bargholtz, R.E. Ekström, K. Fransson, B. Ritzén and P.-E. Tegnér, Nucl. Phys. A464(1987)430

[12] M. Thoennessen, D.R. Chakrabarty, M.G. Herman, R. Butsch and P. Paul, Phys. Rev. Lett. 59(1987)2860

[13] D.R. Chakrabarty, Nucl. Phys. A482(1988)81c

[14] A. Gavron, A. Gayer, J. Boissevain, H.C. Britt, T.C. Awes, J.R. Beene, B. Cheynis, D. Drain, R.L. Ferguson, F.E. Obenshain, F. Plasil, G.R. Young, G.A. Petitt and C. Butler, Phys. Rev. C35(1987)579.

FIGURE CAPTIONS

Fig. 1. Ion-ion potentials calculated in the sudden approximation for orbital angular momentum L=0 (full-drawn) and L=20 (dashed).

Fig. 2. Spectrum of the molecular excitations calculated for the carbon-terbium system.

Fig. 3. The approximative gamma-ray energy of the $\nu = 1 \rightarrow \nu = 0$, L = 15 transition for different target/beam combinations. Note that, in the calculation, an effective mass of 1.0 was used for the lighter mass partner (A_1).

Fig. 4. The driving potentials for the $^{12}C+^{159}Tb$ system. The potential for the ν=2, L=15 state is shown full-drawn, the potential of the ν=0 L=30 state is dashed and the potential of ν=0 L=15 state is dotted.

Fig. 5. Time development of the mass asymmetry of the $^{12}C+^{159}Tb$ system for the ν=2,L=15 state.

Fig. 6. Measured gamma-ray spectrum following the $^{12}C+^{159}Tb$ reaction, (from [11]), and the calculated spectrum of dinuclear transitions (dashed).

Fig. 7. Directional correlation coefficient A_2 for gamma-rays following the $^{12}C+^{159}Tb$ reaction at 100 MeV. The experimental results (points) are well reproduced by the calculation (full-drawn).

Fig. 8. Measured and calculated gamma-ray spectra for the $^{16}O+^{208}Pb$ reaction. The dashed line is the spectrum of gamma rays from molecular transitions. The statistical gamma-ray spectrum emitted from the compound nucleus and the hot fission fragments, dashed-dotted, is taken to be that calculated in ref. [12] assuming no fission hindrance. Adding the spectrum of molecular transitions to the statistical spectrum, one obtains the full-drawn line for the total gamma-ray spectrum, to be compared to the measured spectrum(from [12]), the dotted line.

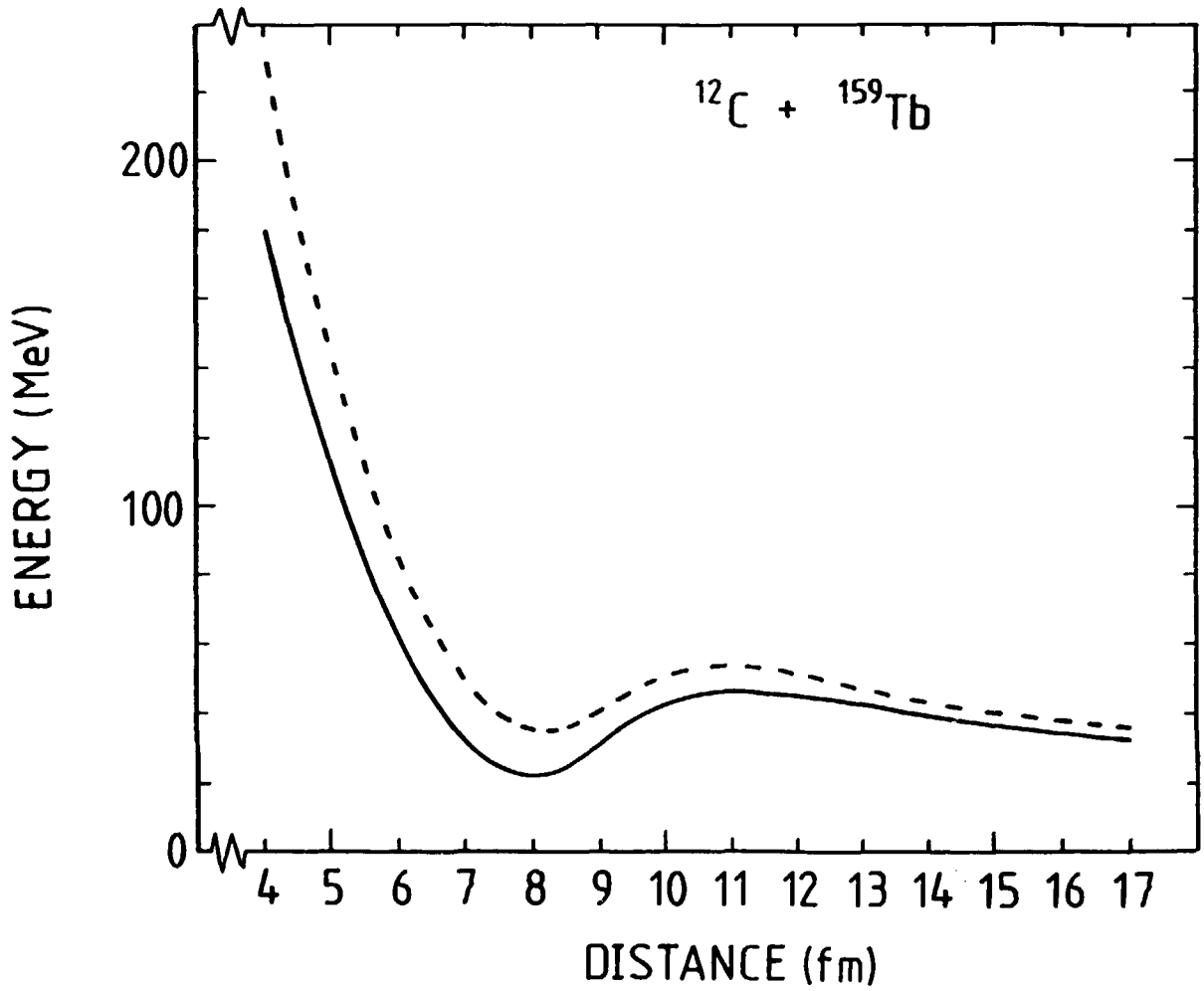
^{12}C + ^{159}Tb
200
100
0
ENERGY (MeV)
4 5 6 7 8 9 10 11 12 13 14 15 16 17
DISTANCE (fm)

FIG. 1

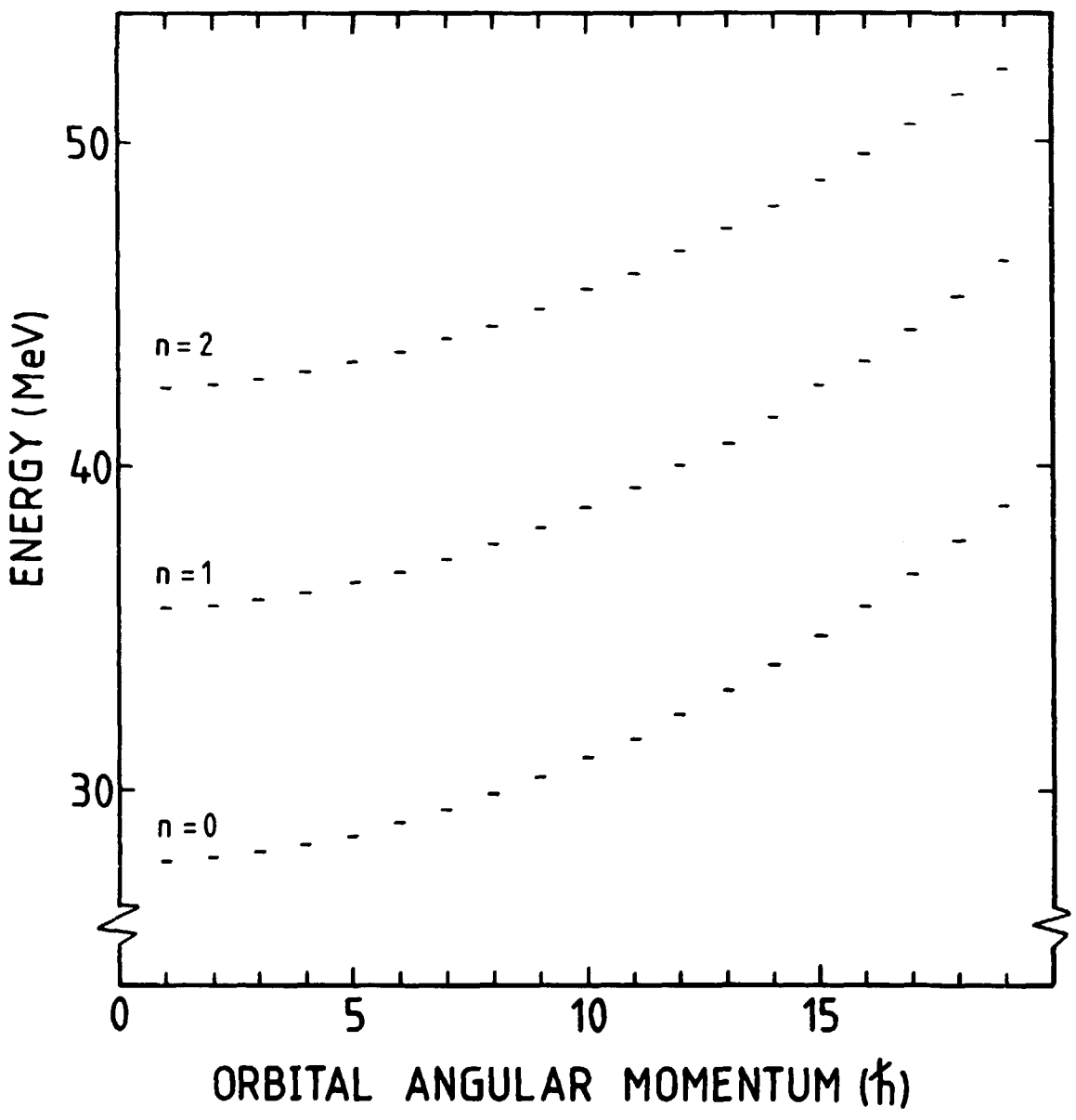
50
40
30
ENERGY (MeV)
n = 2
n = 1
n = 0
0
5
10
15
ORBITAL ANGULAR MOMENTUM (ħ)

FIG. 2

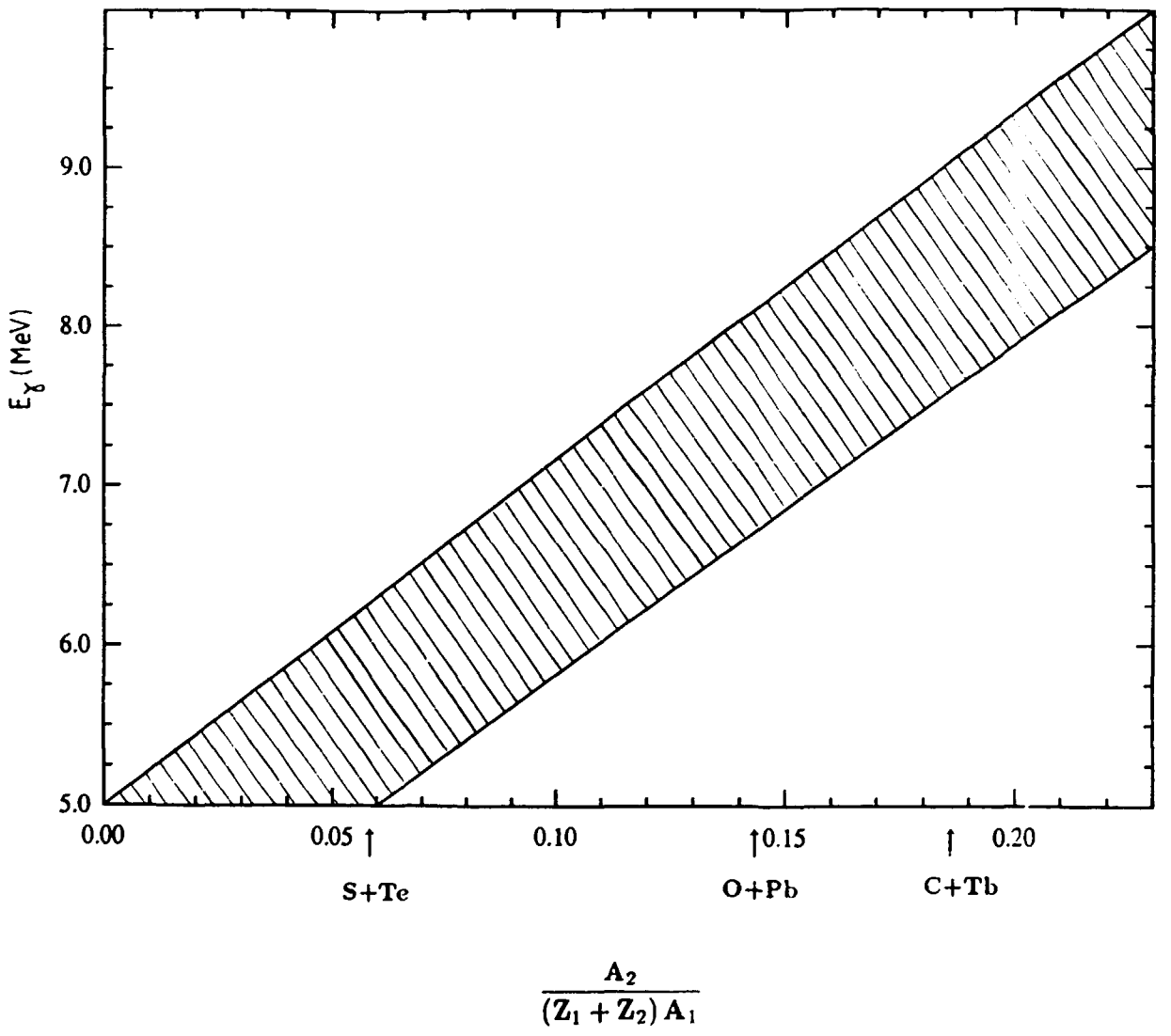
9.0
8.0
7.0
6.0
5.0
E_γ (MeV)
0.00
0.05
0.10
0.15
0.20
S+Te
O+Pb
C+Tb
$\frac{A_2}{(Z_1 + Z_2) A_1}$

FIG. 3

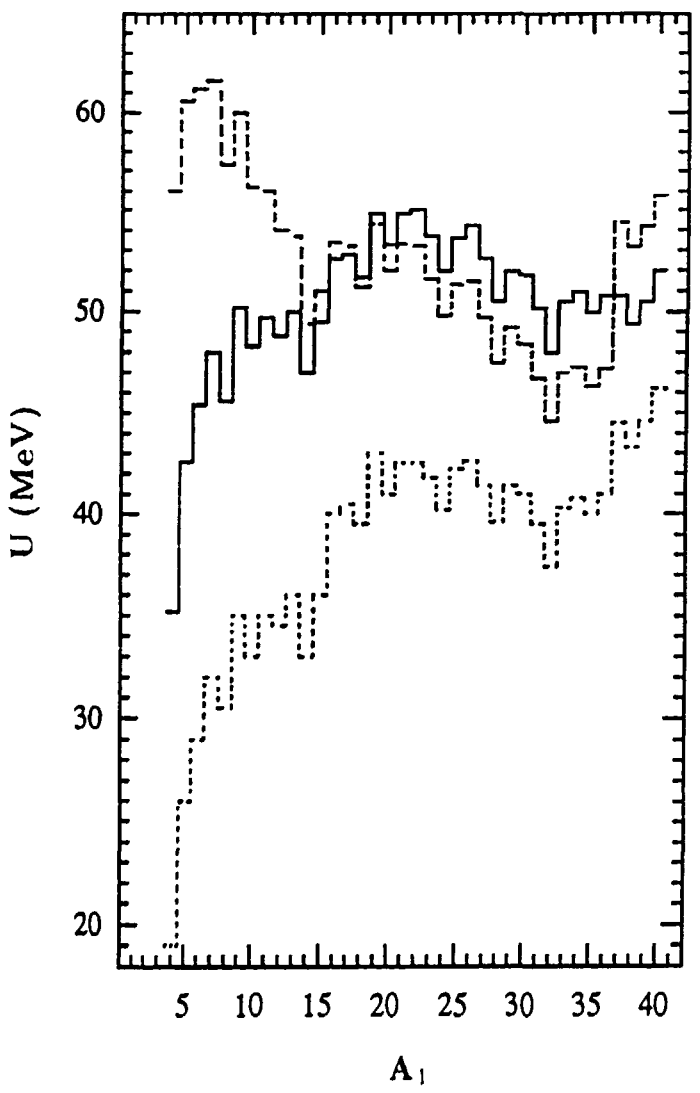

FIG. 4

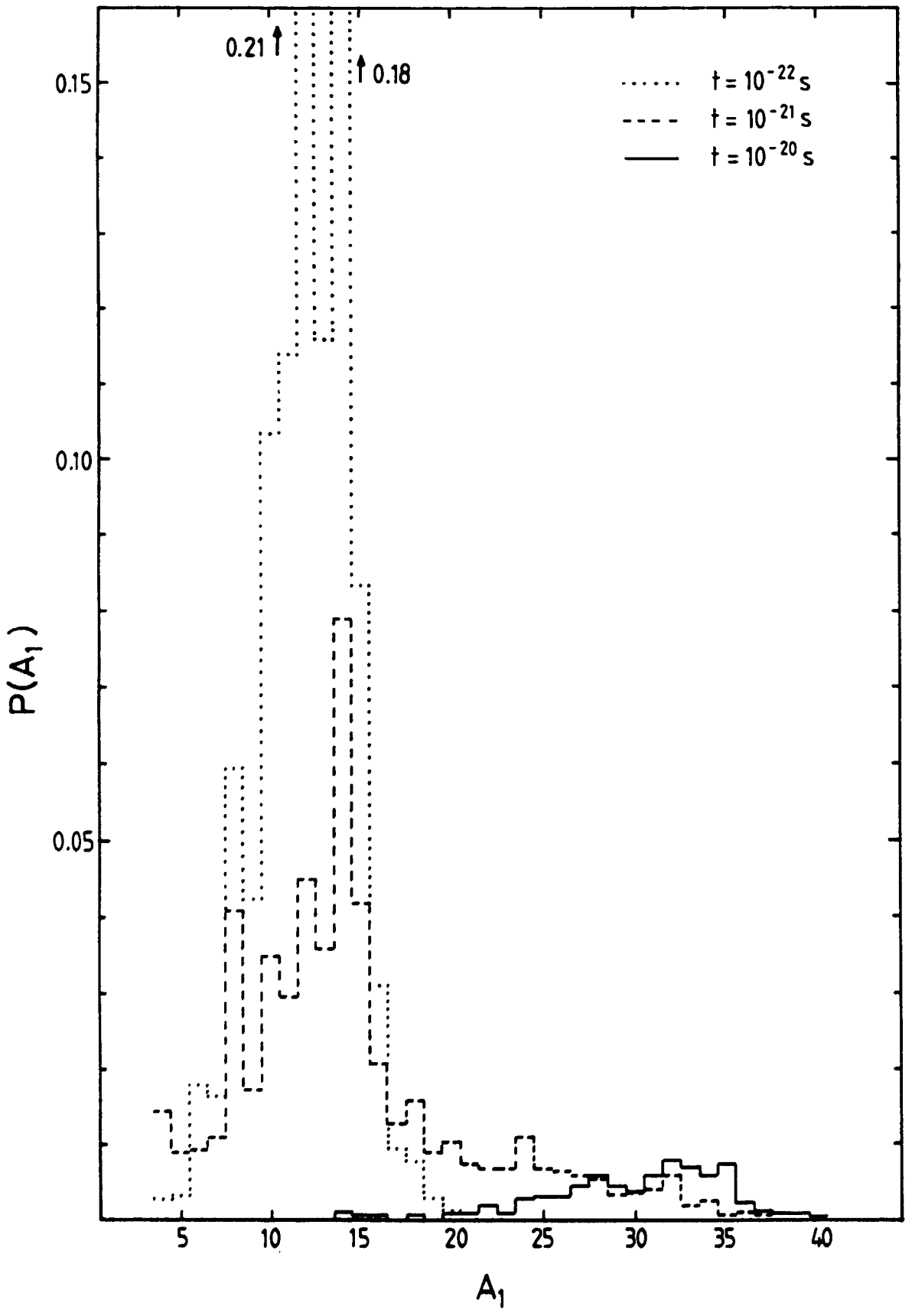
0.21
0.18
0.15
0.10
0.05
P(A1)
t = 10^-22 s
t = 10^-21 s
t = 10^-20 s
5
10
15
20
25
30
35
40
A1

FIG. 5

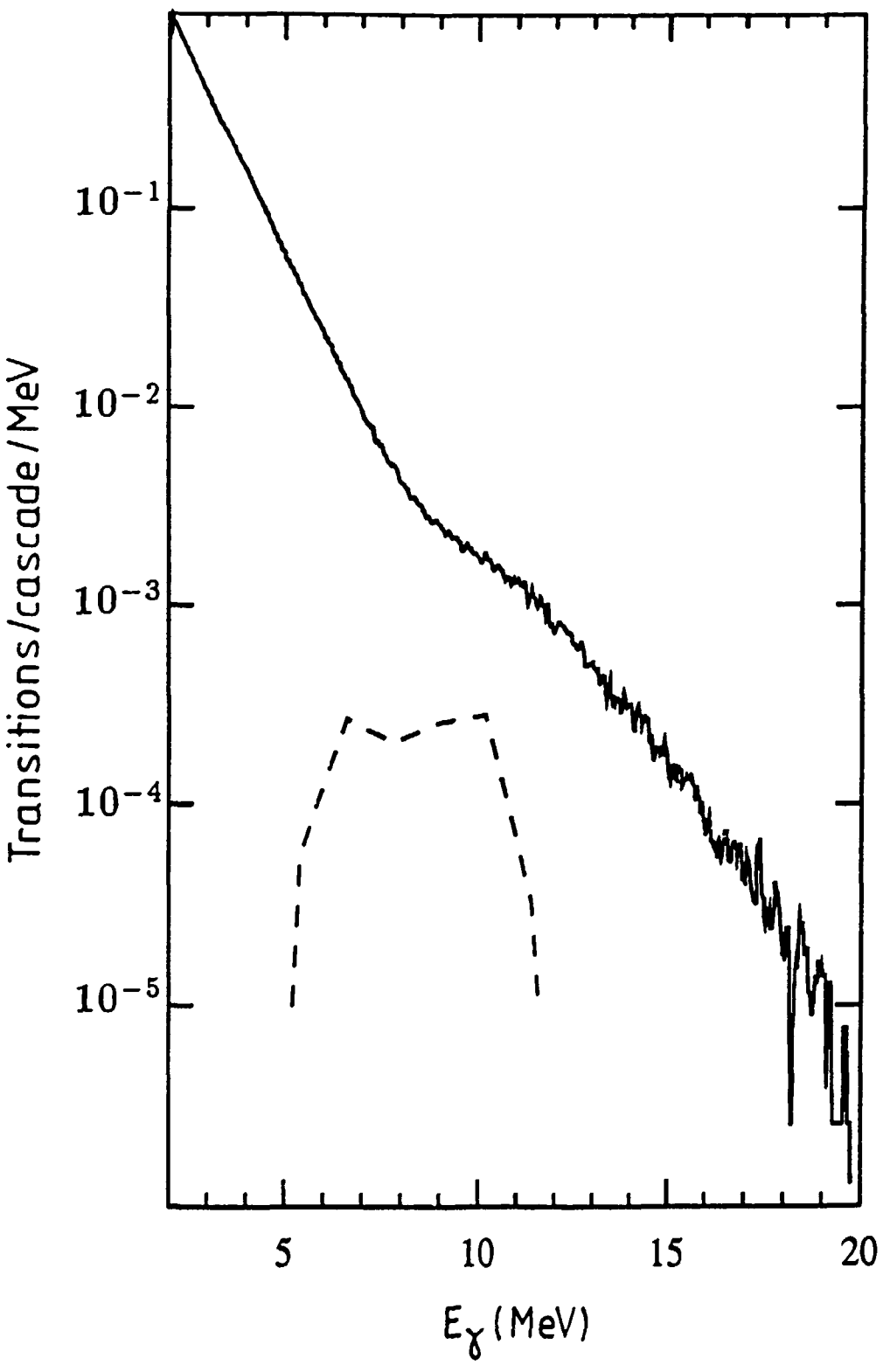
Transitions/cascade/MeV
10^{-1}
10^{-2}
10^{-3}
10^{-4}
10^{-5}
5
10
15
20
E_γ (MeV)

FIG. 6

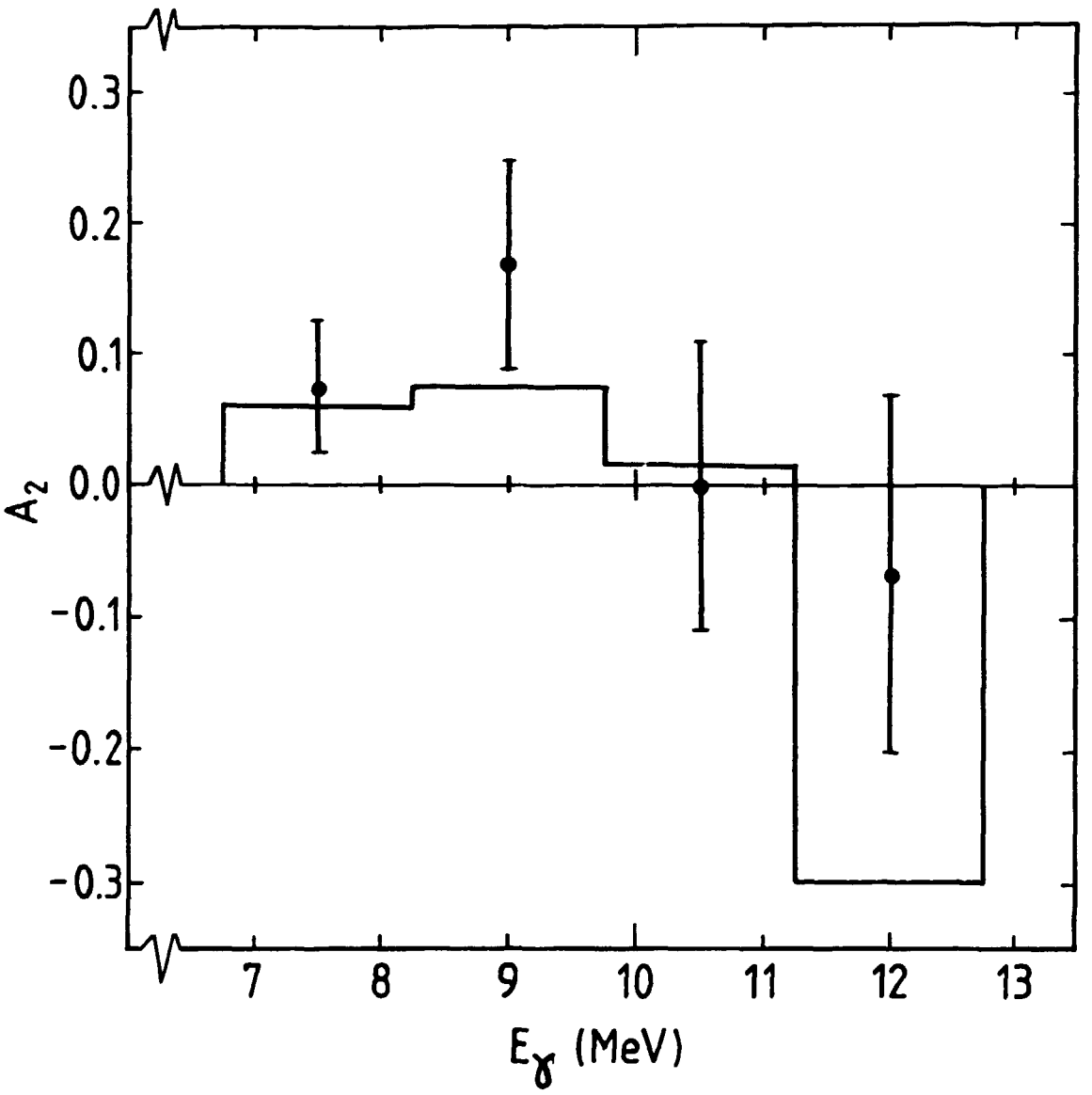

FIG. 7

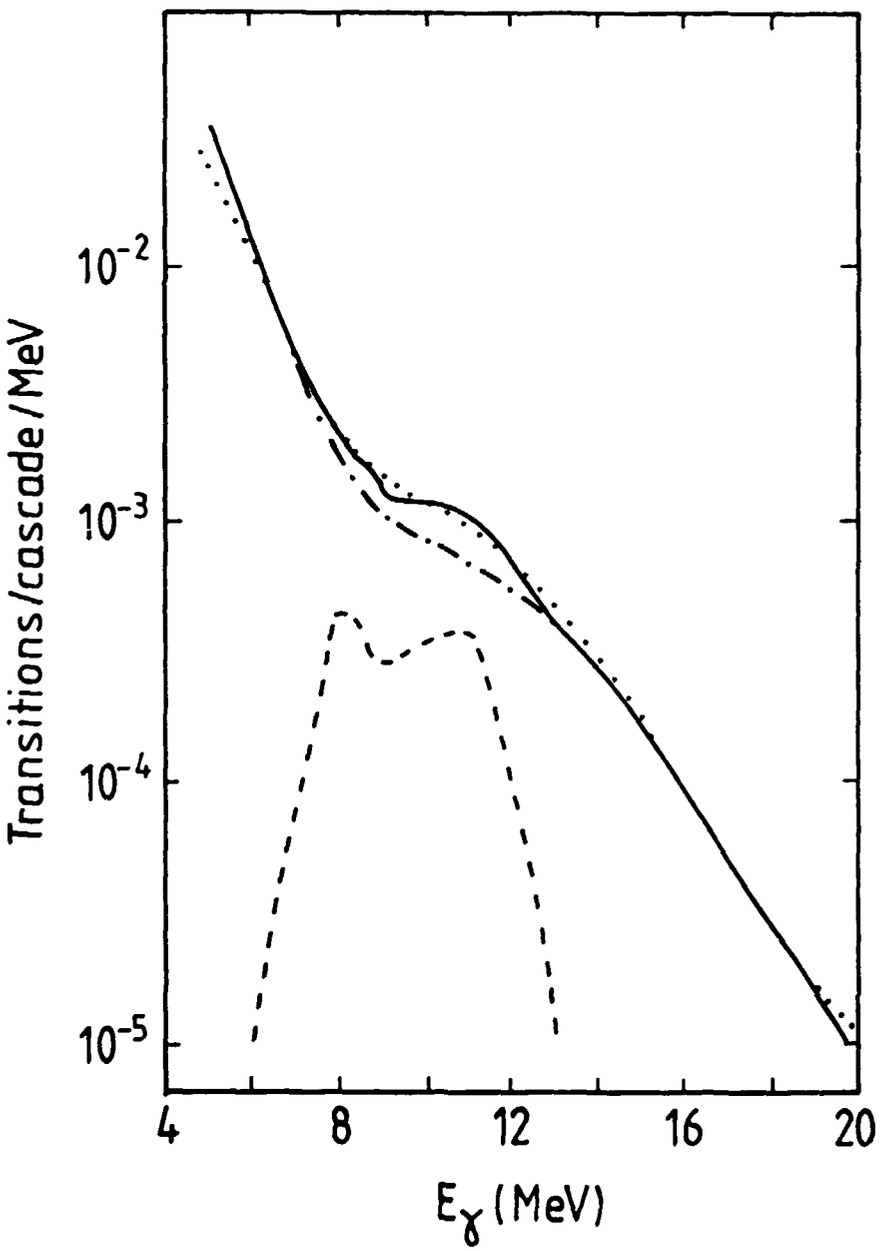
Transitions/cascade/MeV
10^{-2}
10^{-3}
10^{-4}
10^{-5}
4
8
12
16
20
E_γ (MeV)

FIG. 8